Available online at www.sciencedirect.com
ScienceDirect
Archives of Biochemistry and Biophysics 470 (2008) 54–63
ABB
www.elsevier.com/locate/yabbi

A comparative molecular dynamics analysis of the amyloid β-peptide in a lipid bilayer

Justin A. Lemkul, David R. Bevan *

Department of Biochemistry, Virginia Polytechnic Institute and State University, West Campus Drive, 201 Fralin Biotechnology Center, Blacksburg, VA 24061, USA

Received 11 October 2007, and in revised form 6 November 2007
Available online 17 November 2007

Abstract

Because the amyloid β-peptide (Aβ) functions as approximately half of the transmembrane domain of the amyloid precursor protein and interaction of Aβ with membranes is proposed to result in neurotoxicity, the association of Aβ with membranes likely is important in the etiology of Alzheimer's disease. Atomic details of the interaction of Aβ with membranes are not accessible with most experimental techniques, but computational methods can provide this information. Here, we present the results of ten 100-ns molecular dynamics (MD) simulations of the 40-residue amyloid β-peptide ($A\beta_{40}$) embedded in a dipalmitoylphosphatidylcholine (DPPC) bilayer. The present study examines the effects of insertion depth, protonation state of key residues, and ionic strength on $A\beta_{40}$ in a DPPC bilayer. In all cases, a portion of the peptide remained embedded in the bilayer. In the case of deeper insertion depth, $A\beta_{40}$ adopted a near-transmembrane orientation, drawing water molecules into the bilayer to associate with its charged amino acids. In the case of shallower insertion, the most widely-accepted construct, the peptide associated strongly with the membrane–water interface and the phosphatidylcholine headgroups of the bilayer. In most cases, significant disordering of the extracellular segment of the peptide was observed, and the brief appearance of a β-strand was noted in one case. Our results compare well with a variety of experimental and computational findings. From this study, we conclude that Aβ associated with membranes is dynamic and capable of adopting a number of conformations, each of which may have significance in understanding the progression of Alzheimer's disease.

Keywords: Alzheimer's; Amyloid; Molecular dynamics; Protein–lipid interactions

Alzheimer's disease is a progressive, neurodegenerative disorder characterized by cognitive decline and dementia [1]. According to recent estimates by the Alzheimer's Association [2], there are currently 5.1 million Americans with Alzheimer's, and a 50% increase in cases in individuals over the age of 65 is expected to occur by the year 2030. By 2050, the number of cases could be as high as 16 million, according to current predictions. Nationwide, Alzheimer's causes deaths at a rate of nearly 22 per 100,000 population.

A hallmark of Alzheimer's disease is the formation of extracellular neuritic plaques [3], the core of which is formed by amyloid β-peptides (Aβ).[1] These Aβ peptides, which can range in length from 39 to 43 amino acids, are derived from sequential proteolytic cleavage of the amyloid precursor protein (APP) by β-secretase activity at its N-terminus and γ-secretase within the membrane [3]. The toxic effects seen in Alzheimer's disease are thought to arise as a result of the conformational changes in Aβ from predominantly α-helical to a mixture of folding intermediates rich in β-structures that lead to fibril formation [4–7]. Experimental and computational methods have successfully been

* Corresponding author. Fax: +1 540 231 9070.
E-mail address: drbevan@vt.edu (D.R. Bevan).

[1] *Abbreviations used:* Aβ, amyloid β-peptides; APP, amyloid precursor protein; CTF, C-terminal fragment; DMPC, dimyristoylphosphatidylcholine; DPPC, dipalmitoylphosphatidylcholine.

0003-9861/$ - see front matter © 2007 Elsevier Inc. All rights reserved.
doi:10.1016/j.abb.2007.11.004

used to provide detailed information on the structure of amyloid fibrils and intermediate assemblies [8–12].

Experiments have shed light on the structure of $A\beta_{40}$ and its position within the membrane [13]. The peptide has been found to be mostly α-helical in a membrane-mimicking environment, and its C-terminal helix is thought to be embedded in the lipid bilayer [14]. In a previous MD study on $A\beta_{40}$, Lys-28 was assigned to the interface region between the bilayer and the aqueous environment [15]. That study found that $A\beta_{40}$ exited a DPPC bilayer within a 100-ns MD timeframe and much of the α-helical character of the peptide was retained throughout the simulation. While a number of theoretical studies have been conducted on Aβ [15–21], the Xu et al. [15] study is the only one to our knowledge that has previously examined $A\beta_{40}$ in an explicit bilayer environment.

There is evidence to suggest that $A\beta_{40}$ is positioned in the membrane such that Val-24 is located at the interface, instead of Lys-28. An early study suggested that in the 99-residue C-terminal fragment (CTF), the peptide derived by β-secretase cleavage and prior to γ-secretase cleavage, Val-46 (numbered such that Asp-1 in Aβ is also Asp-1 in CTF) is located within the membrane on the intracellular side of the bilayer. This places the lysine triplet at residues 53–55 slightly away from the interface [22]. In 1998, Coles and colleagues proposed a number of possibilities for the location of Aβ within the plasma membrane based on the structure they solved [14]. Given this structure, if Lys-53–Lys-55 were located where Tischer and Cordell [22] predicted them to be, Val-24 would be positioned at the interface. The insertion depth of Aβ within a lipid bilayer could have important implications for its mechanism of exit and its propensity to do so.

An *in vitro* study of rat synaptic plasma membranes showed that Aβ peptides intercalated in the membrane [23]. That study found that soluble Aβ monomers were capable of penetrating deep into the bilayer core, whereas aggregates were found closer to the interface region. The peptides were found to reduce membrane thickness, of possible implication in the pathology of Alzheimer's. This insertion phenomenon has been shown to be strongly influenced by pH and the presence of metal ions, specifically Cu^{2+} and Zn^{2+} [24].

A later study by Yip and McLaurin used atomic-force microscopy to find that $A\beta_{40}$ monomers were partially inserted into lipid bilayers rather than fully embedded in the bilayer core [25]. Furthermore, that study found that Aβ adopted a mostly random conformation in the presence of dimyristoylphosphatidylcholine (DMPC) micelles, which have zwitterionic headgroups. Fibrils were observed to form within the lipid headgroups, leading the authors to hypothesize that this fibril formation caused membrane disruption and overall loss of integrity. These observations have implications regarding ionic balance across lipid bilayers in Alzheimer's patients. It is well-known that Aβ causes disruption of the ionic balance across neural cell membranes [26,27], but the exact mechanism of this disruption has not been determined. Increased ion conductance across cell membranes has been observed in the presence of Aβ oligomers, which associate at the bilayer periphery [28]. This phenomenon was not observed when only soluble Aβ monomers were present. Another study observed that $A\beta_{40}$ oligomers led to increased intracellular Ca^{2+} levels, which could signal apoptotic pathways [29].

The interactions between $A\beta_{40}$ and the lipid bilayer are primarily due to electrostatic and van der Waals forces [15]. A previous MD study showed that the behavior of Aβ fragments in aqueous solution is significantly affected by the presence of ions. It was demonstrated that ions had a pronounced effect on the intra- and inter-peptide interactions thought to be important in Aβ aggregation [30]. The presence of salt, specifically sodium chloride, has also been shown to affect the interactions between charged lipid headgroups [31]. Based on the nature of the interactions between Aβ and the bilayer, it is hypothesized that the presence of a physiologically-relevant salt concentration will affect the behavior of Aβ at the membrane interface.

As a final note, it was shown by Ma et al. that pH plays a major role in the progression of amyloidosis [6]. The protonation states of ionizable sidechains on Aβ have implications on the rate of aggregate formation. The authors used NMR to determine the pK_a values of titratable sidechains in the 28-residue Aβ fragment and summarized the structural implications in different environments and at various pH values.

In this study, we expand upon previous work by using computational methods to examine the effects of pH, insertion depth in the bilayer, ionic strength, and temperature on the behavior of Aβ in a lipid bilayer. These results are interpreted in light of previous computational and experimental studies.

Materials and methods

Determination of pK_a values

Of importance in this study was the protonation state of certain amino acid residues of Aβ in both aqueous and membrane environments. To determine the pK_a values of the titratable residues in $A\beta_{40}$, the structure file (PDB entry 1BA4 [14], the fourth of 10 NMR structures determined at pH 5.1 in the presence of SDS micelles) was submitted to Virginia Tech's H++ server [32,33]. This structure was chosen because its conformation was such that its N-terminal loop would not be initially located within or near the bilayer after insertion. Our simulations involved three models based on insertion depth—Models A and B located Lys-28 at the interface, while Model C located Val-24 at the interface. For pK_a calculations, the Aβ structure was separated into two parts, the segment of the peptide that would be exposed to an aqueous environment (residues 1–28 in Models A and B; residues 1–24 in Model C), and that which would be embedded in the bilayer (residues 29–40 in Models A and B; residues 25–40 in Model C). For the aqueous segment, calculations were performed using an internal dielectric of 6 [34], external dielectric of 80 [34], ionic strength of 0.10 M, and a pH of 7 for Models A and C, and pH 5.1 for Model B. For the membrane-bound segment, calculations were performed with an internal dielectric of 6 [34], external dielectric of 2 [35,36], ionic strength of 0 M, and pH of 7 to simulate a bilayer environment.

To account for the dielectric continuum that exists within a DPPC bilayer [35,36], calculations were repeated on the membrane-bound segment of $A\beta_{40}$ to verify the protonation states of Lys-28 and the C-terminus in Model C. External dielectric values were varied from 3 to 10 to monitor the change in pK_a value of these residues throughout the entirety of the DPPC bilayer. The internal dielectric was maintained at 6 for all calculations.

Construction of $A\beta_{40}$/bilayer systems

A total of 10 systems were prepared. Eight systems located Lys-28 at the water–bilayer interface (Models A and B). Of these eight, four had deprotonated C-termini (A1, A2, B1, and B2—see Table 1), and four were protonated (A3, A4, B3, and B4). Model A systems were prepared either with only enough counterions to give the system a net charge of zero (neutralizing counterions) or with ~100 mM NaCl. Model B systems were prepared with only neutralizing counterions. The remaining two models located Val-24 at the interface (Model C) with neutralizing counterions only and ~100 mM NaCl. Both of these models had deprotonated C-termini. All preparation steps, minimizations, equilibrations, and production MD runs were conducted using facilities provided within the Gromacs package, version 3.3 [37,38], or scripts written in-house.

The $A\beta_{40}$ peptide was solvated within a 6.5-nm cubic box of simple point charge (SPC) water and submitted for energy minimization. Water molecules were removed from the output structure to give the peptide that was used to construct the peptide/bilayer systems.

Structure and topology files for a pre-equilibrated, 128-lipid DPPC bilayer solvated with 3655 water molecules were downloaded from the Tieleman group's website [39]. DPPC was chosen because it was used in a previous MD study [15], and it closely resembles systems used experimentally, such as DMPC and dodecylphosphocholine (DPC) micelles [6,25], in terms of surface charge and lipid composition. To construct the peptide/bilayer systems, a Perl script was used to overlap the coordinate files of the peptide and the DPPC bilayer and delete DPPC residues that had atoms within 1.3 Å of the peptide, such that any bad contacts at 1.4 Å could be resolved by energy minimization. The output structure was submitted for energy minimization, first with position restraints on $A\beta_{40}$ ($k_{pr} = 1000\ kJ\ mol^{-1}\ nm^{-2}$), and again without these restraints. The peptide/bilayer system was solvated by adding a slab of water to the extracellular face of the bilayer. This step was done to solvate the peptide and provide additional room for any potential movements of the N-terminal loop segment. The system was energy-minimized, after which counterions were added to compensate for the net charge on the system. To the systems with higher ionic strength, additional sodium and chloride ions were added. Minimizations were performed after each addition of ions. Box dimensions following construction of the system were 6.5 nm in the lateral directions, with a height of approximately 10 nm.

Equilibration of the solvated $A\beta_{40}$/bilayer system

Each system was equilibrated in two steps over a total of 600 ps. Position restraints were placed on the bilayer headgroups and the peptide during both procedures, using the same spring constant as in position-restrained minimization, discussed above. A 100-ps NVT simulation was conducted using the Berendsen temperature coupling method [40] with a temperature coupling constant (τ_T) of 0.1 ps. Each group (peptide, lipids, solvent/ions) was coupled to a separate temperature bath. The parameters developed and employed by Tieleman were applied to the DPPC bilayer [41–43], and the Gromos96 53a6 force field [44] was applied to the rest of the system. This procedure is quite similar to other previously reported methods [15,45–51]. Electrostatic interactions were calculated using the Particle Mesh Ewald (PME) method [52,53] with a fourth-order spline interpolation and Fourier grid spacing of 0.12 nm. The linear constraint solver (Lincs) method [54] was used to constrain all bond lengths, with a 2-fs integration step. Operations were carried out on Virginia Tech's 1100-node SystemX Apple Xserve G5-based supercomputer (2.3 GHz PowerPC 970FX processors) [55].

Following the NVT simulation, NPT conditions were imposed. The previous parameters were employed, and pressures were applied independently in the x, y, and z directions using the Berendsen method [40]. To pack the lipids around the peptide and accelerate equilibration, a pressure of 100.0 bar was applied in the transverse direction, and 1.0 bar in the vertical direction. A pressure coupling constant (τ_P) of 2.0 ps was used [56,57], and the operation was carried out over 500 ps. At the conclusion of the equilibration steps, the box was a 6-nm square in the lateral direction, with a height of approximately 10 nm.

Models A1–A2 and C1–C2 are likely the most physiologically-relevant, as they have the same protonation state based on pH 7 calculations; these sets differ only in insertion depth. Models A3 and A4 are used to examine the effects of a protonated C-terminus on the conformational changes of $A\beta_{40}$. Models B1 and B2 represent the peptide at pH 5.1, while Models B3 and B4 correspond to the peptide at a pH such that all titratable residues would be protonated. Although not likely to be physiologically-relevant in a membrane environment, these models allow us to examine the effects of protonation state on the interactions of Aβ with the bilayer.

Molecular dynamics simulations

A total of 100 ns of MD were performed on each system following the equilibration described above. Pressure was set at 1.0 bar in all directions. During production MD, temperature and pressure were regulated using a weak coupling method ($\tau_T = 0.1$ ps and $\tau_P = 2.0$ ps) [40,56,57]. All analyses were performed using facilities within the Gromacs package and the DSSP program [58]. Images of the $A\beta_{40}$/bilayer system were generated with UCSF Chimera [59].

Table 1
Simulation systems

Model	Ionic strength (mM)	DPPC lipids	Peptide net charge	Temperature (K)	Na^+ ions	Cl^- ions	H_2O molecules	Simulation ID
A	0*	122	–3	323	3	0	6912	A1
	100		–3		26	23	6873	A2
	0		–2		2	0	6922	A3
	100		–2		26	24	6878	A4
B	0	122	+1	300	0	1	6949	B1
	0		+1	323	0	1	6948	B2
	0		+7	300	0	7	6951	B3
	0		+7	323	0	7	6948	B4
C	0	120	–3	323	3	0	6928	C1
	100		–3		26	23	6888	C2

*An ionic strength of zero implies counterions sufficient to neutralize the charge on the peptide.

Results

pK_a calculations

Results of H++ calculations are presented in Table 2. All models are predicted to have deprotonated C-termini, based on the very low pK_a values of these residues. The only other pK_a value that is shifted relative to the canonical value is that of Lys-28 in Model C, which is elevated, and indicates that the residue is likely to be protonated under the given conditions, just as it is in the other models. All other residues have nearly canonical pK_a values. The results of these calculations compare well with the findings of Ma et al. [6]. While not perfectly matched, these calculated pK_a values lead to the same protonation state predicted by Ma et al. at physiological pH.

In Model C, both Lys-28 and the C-terminal valine are embedded in the DPPC bilayer, but due to the dielectric continuum previously described, these residues do not experience the same dielectric environment. Thus, calculations were repeated as discussed above (see Materials and methods). The pK_a values for Lys-28 remain above 11, and those for the C-terminus remain below 3, and thus the calculations predict that Lys-28 will be protonated, and the C-terminus, deprotonated at all points within the DPPC bilayer.

Molecular dynamics simulations

Starting structures for each of the models are shown in Fig. 1a and b. Structures at the end of the simulations are illustrated in Fig. 1c–l. These images from the end of the trajectory provide representative structures, as few major conformational changes were observed after 50 ns of simulation. A description of the observations from the simulations is given below. The following terminology will be used to refer to various segments of the Aβ_{40} peptide: N-terminal loop (residues 1–14), helix 1 (residues 15–24), hinge region (residues 25–27), helix 2 (residues 28–36), and C-terminal loop (residues 37–40).

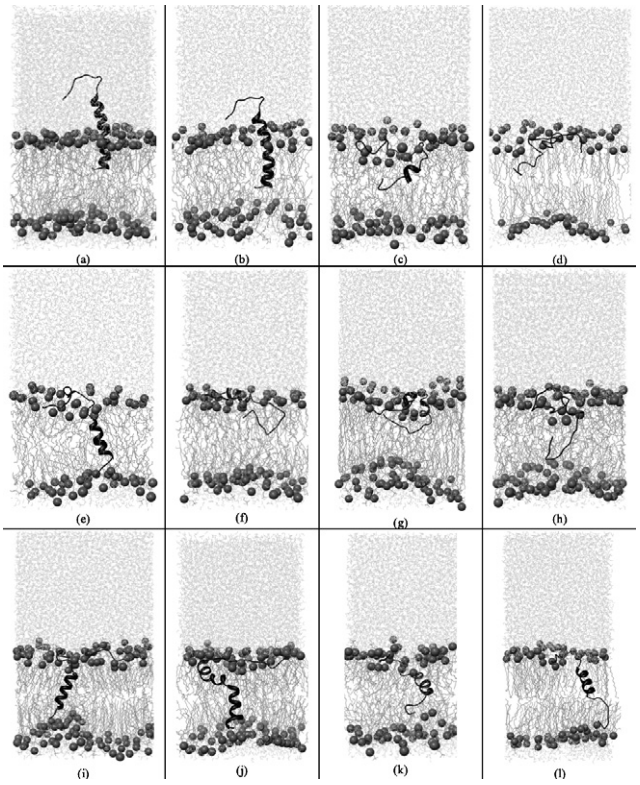

Fig. 1. Structures from all trajectories: (a) starting structure of Models A and B; (b) starting structure of Model C; (c–l) structures after 100 ns, which are representative of the trajectory: (c) A1, (d) A2, (e) A3, (f) A4, (g) B1, (h) B2, (i) B3, (j) B4, (k) C1, and (l) C2. The peptide is rendered as a ribbon, the DPPC bilayer as sticks with phosphorus atoms shown as spheres, and water molecules are shown as lines. Some DPPC molecules were deleted from in front of the peptide for clarity.

Table 2
pK_a values, as calculated by H++

Residue	Model A	Model B	Model C	Charge state at pH 7	Charge state at pH 5.1
N-terminus	8.4	9.0	8.4	+	+
Asp-1	1.7	0.3	1.7	−	−
Glu-3	4.0	3.6	4.0	−	−
Arg-5	12.5	13.4	12.6	+	+
His-6	6.8	7.0	6.8	0[a]	+
Asp-7	3.6	2.1	3.6	−	−
Tyr-10	11.5	12.3	11.5	0	0
Glu-11	4.6	4.4	4.7	−	−
His-13	6.4	6.5	6.5	0	+
His-14	5.8	5.9	5.8	0	+
Lys-16	10.6	11.4	10.7	+	+
Glu-22	5.6	5.5	5.7	−	0[b]
Asp-23	3.6	2.7	3.9	−	−
Lys-28	10.9	9.9	23.5	+	+
C-terminus	−2.8	−3.2	−3.6	−	−

[a] A charge state of "0" indicates that these residues were in neutral protonation states, although the histidine residues (in all models) are likely to be partially protonated (and thus contribute some positive charge) in an actual physiological system.
[b] Glu-22 (in Model B) is likely to be partially deprotonated at pH 5.1 and contribute some negative charge.

Simulation set A

This simulation set included models of the $A\beta_{40}$ peptide at physiological pH and at two different ionic strengths. These simulations began with a widely-accepted construct for the positioning of the peptide in the membrane, which locates Lys-28 at the water/bilayer interface.

Characteristic in this set of simulations was that $A\beta_{40}$ remained partially embedded in the DPPC bilayer, such that Lys-28 remained at the interface, with the exception of A3, wherein the peptide located itself such that Val-24 was at the interface. Also typical of these simulations was loss of α-helicity in favor of random and β-structures in some portions of the peptides (Fig. 2). For example, in A1, helix 1 lost all α-helicity within approximately 35 ns of simulation, with unwinding initiating at Glu-22 and Asp-23 (both deprotonated), a phenomenon predicted by Coles et al. [14]. Simulation A2 featured a complete loss of α-helicity within the first 10 ns of simulation, but was similar to A1 in that the peptide was located similarly within the bilayer. Simulation A3 differed from the other simulations in this group in that a central segment of this peptide retained its original α-helicity. Finally, the peptide in A4 was similar in position to A1 and A2, but retained α-helicity in helix 1. The positioning of A3 likely results from the increased hydrophobicity of its C-terminus by virtue of its protonation. The peptide in A4 also had a protonated C-terminus, but may have been attracted more strongly to the aqueous environment due to the increased ionic strength.

Presence of Aβ at the interface and the unwinding events we observed are in good agreement with the findings of Yip and McLaurin [25]. Simulation A3 agrees with experimental evidence that suggests Aβ monomers are capable of penetrating the hydrophobic core of a lipid bilayer [23]. These findings differ from those of a similar work, wherein $A\beta_{40}$ exited a DPPC bilayer within 100 ns and maintained much of its original α-helicity [15].

Simulation set B

This simulation set was designed to examine the effects of protonation state (pH) and temperature, above and below the phase-transition temperature for DPPC, on the behavior of $A\beta_{40}$ and the surrounding lipid environment. The low pH environment is unrepresentative of the plasma membrane, but resembles that of the endosomal membrane environment and enables us to study the sensitivity of Aβ-membrane interactions to changing protonation state.

None of the peptides in this simulation set exited the bilayer, and no β-strands were observed, but other β-structures developed over time (Fig. 2). Simulation B1 featured two short segments that retained α-helicity throughout 100 ns. Simulation B2, carried out at a higher temperature, showed similar helical features, but helicity in residues 15–20 eventually disappeared over time. The $A\beta_{40}$ peptide in

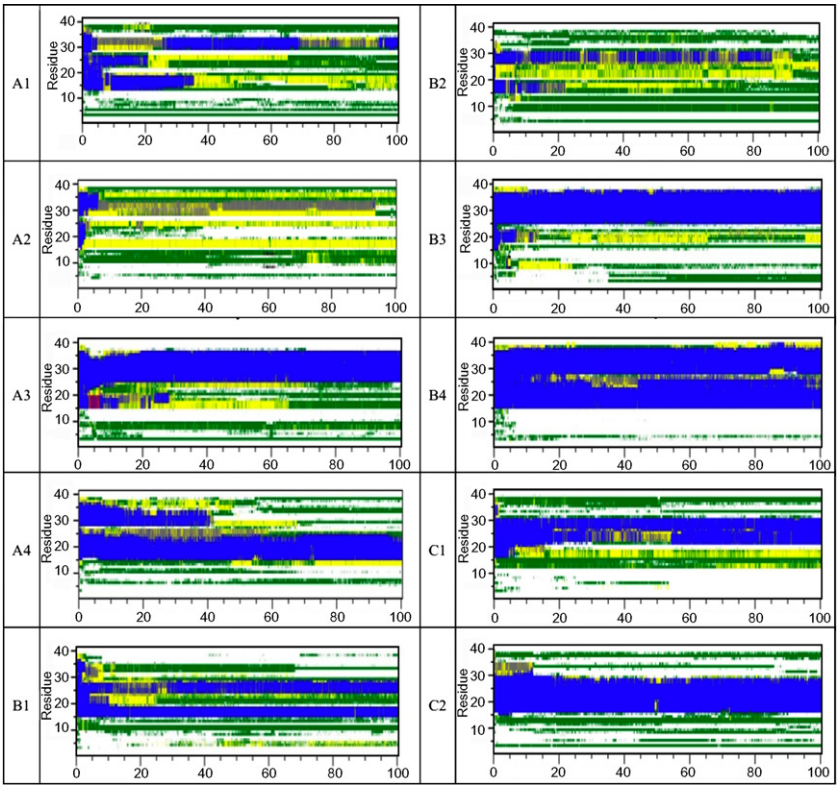

Fig. 2. Secondary structure analysis for all trajectories. The *x*-axis in each diagram represents time in nanoseconds. Legend: white—coil, black—β-bridge, green—β-bend, yellow—β-turn, red—β-strand, blue—α-helix, purple—5-helix (π-helix), gray—3_{10}-helix.

both B1 and B2 adopted positioning that placed Val-24 at the interface, slightly deeper than the prevailing positioning in simulation set A. In simulations B3 and B4, in which all ionizable residues in $A\beta_{40}$ were protonated, the peptide became embedded even more deeply within the DPPC bilayer, such that Lys-16 was at the interface throughout most of the trajectory. These peptides retained an appreciable amount of the original α-helical content and adopted nearly transmembrane orientations by the end of 100 ns.

The simulations conducted at 300 K, below the phase-transition temperature of DPPC (B1 and B3), clearly show the effects of the peptide on the surrounding lipids. While DPPC residues far from the peptide tended to extend their acyl chains and pack together, those near the peptide are noticeably more disordered, clearly showing a disruptive effect of the peptide on the surrounding membrane environment.

Increased α-helicity as pH decreases has been observed experimentally [6,14], and we have succeeded in simulating these observations. The NMR data from Coles et al. predicted α-helicity in residues 15–36, broken only by a hinge at residues 25–27 [14]. In simulations B1 and B2, conducted at a simulated pH that mimicked those of the experiment, we observed retention of helicity in residues 15–30, broken by the same hinge. Some α-helicity was lost in B2, likely due to the higher temperature of the simulation (323 K). The structural determination by Coles et al. was conducted at 298 K, slightly lower than the temperature of B1, and much lower than that of B2.

Simulation set C

The purpose of the final two simulations was to monitor the effects of deeper initial insertion depth of $A\beta_{40}$ in the bilayer, a less widely-accepted construct that has some experimental backing. In this simulation set, we examine the effects of initial insertion depth and ionic strength on a system under physiologically-relevant pH and ionic strength.

The peptides in both of these trajectories positioned themselves within the bilayer such that Lys-16 was at the interface, an orientation that was maintained throughout the trajectory. Both simulations featured peptides that retained α-helicity in a central segment (Fig. 2), with the increased ionic strength of C2 having no obvious effect on the behavior of the peptide. Positioning of the Aβ peptide in the core of the bilayer is in good agreement with the findings of Mason et al. [23]. We observed no β-strand

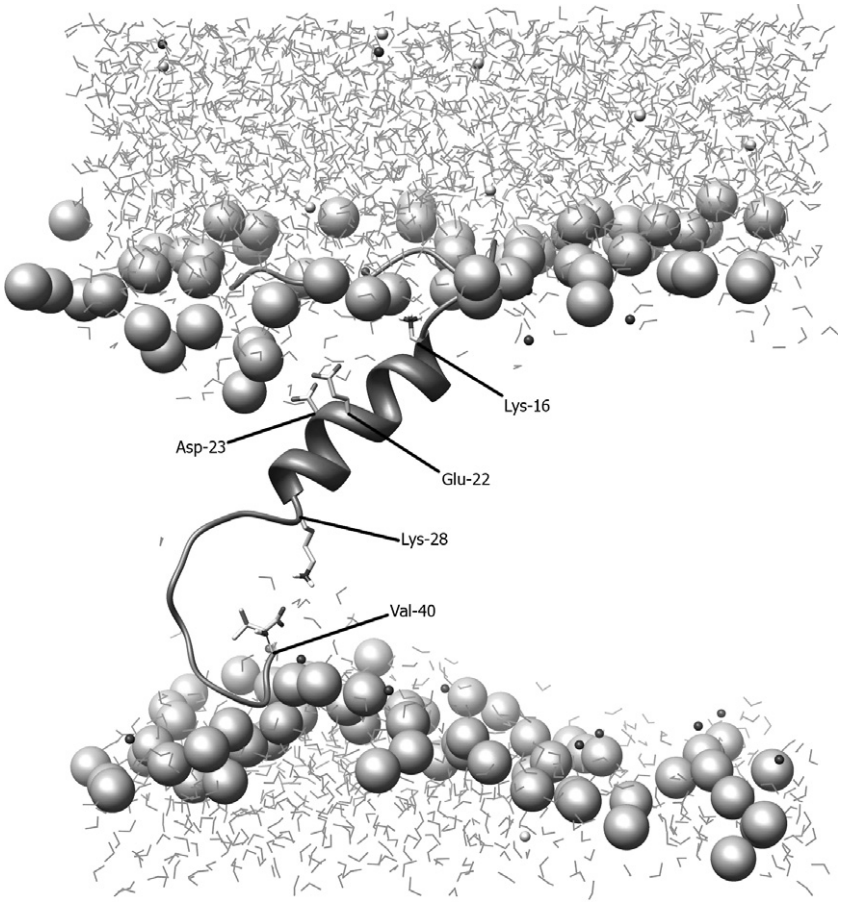

Fig. 3. Water leakage into the lipid bilayer, illustrated using a snapshot at 80 ns. The bilayer has been removed for clarity, but phosphorus atoms are shown as large spheres for perspective. The peptide is shown as a ribbon, with charged sidechains labeled and shown in sticks. Water molecules are shown as lines and ions are shown as small spheres.

structures in either trajectory, and the peptide did not exit the bilayer in the 100-ns timeframe.

An interesting phenomenon that occurred in both C1 and C2 was the persistence of water in the bilayer (Fig. 3). Water molecules entered the bilayer and associated with the four charged groups in the hydrophobic interior (Glu-22, Asp-23, Lys-28, and the C-terminus). This observation is similar to one made in an MD study of melittin [60], where water was thought to enter the bilayer and compromise the integrity of the membrane. This event compares well with experimental observations that membranes are disrupted in the presence of Aβ [61].

The behavior of the charged residues within the hydrophobic interior of the lipid bilayer is worth noting. The presence of charged residues within a lipid bilayer during simulations is not unprecedented. As can be seen from Fig. 3, these charged residues appear to be capable of "snorkeling" to the interface region, a phenomenon that has been reported in other simulations of transmembrane helices [62–64]. Snorkeling was observed in all of our simulations in which charged residues were located within the core of the bilayer (A3, B3, B4, C1, and C2).

Discussion

In a recent review, Haass and Selkoe present a model for the generation of Aβ from APP that describes the association of Aβ with membrane compartments [65]. Although Aβ is depicted as exiting the membrane after γ-secretase cleavage, no model is yet available to describe the release of Aβ to the extracellular space. To develop a complete understanding of the role of Aβ in Alzheimer's disease, it is necessary to devise studies that consider Aβ in association with membranes. Atomic-level descriptions of Aβ association with lipid bilayers are not currently feasible using experimental methods, though several investigators have examined its structure in the presence of membrane-mimicking environments such as organic solvents, detergents, and phospholipid micelles [6,14,25,66].

Computational methods are applicable to studies of peptide and protein interactions with phospholipid bilayers as models of cell membranes, and a review summarizing some of these studies has recently appeared [67]. Of particular relevance to our work are studies of single helix spanning peptides. For example, early simulation studies utilized melittin in a DPPC bilayer [60,68]. Melittin was inserted in an α-helical conformation with the helix oriented perpendicular to the bilayer surface, but the helix did not completely span the membrane. During the MD simulation, melittin maintained its α-helical conformation, but was observed to adopt a 25° tilt relative to the membrane normal, and a bend of approximately 30° was seen in the helix near the N-terminus, which was the end extending farthest into the bilayer. An MD simulation of alamethicin in a POPC bilayer showed similar results in that a bending motion was observed in the helix, though no appreciable tilt of the peptide was reported [69]. These studies were necessarily short (<2 ns) due to computational resources available at the time. Thus, it is not unexpected that more extensive conformational changes were not observed. More recently, simulations of model $(WALP)_n$ and $(KALP)_n$ transmembrane helices have been done. Kandaswamy and Larson [70] applied MD to studies of $(KALP)_n$ peptides in DLPC, DMPC, and DPPC bilayers, with a particular focus on understanding the effect of hydrophobic mismatch, in which the length of the hydrophobic transmembrane segment varies along with the width of the lipid bilayer. In simulations extending out to 200 ns, they observed that the peptides remained α-helical and that they tilted relative to the bilayer normal when necessary to accommodate the hydrophobic mismatch. Also of relevance are MD studies of the insertion of WALP peptides into membrane environments [71,72]. Both studies started with an extended peptide and applied replica exchange MD to increase conformational sampling, though Im and Brooks [71] utilized a generalized Born implicit membrane model and Nymeyer et al. [72] used an explicit DPPC bilayer. Very distinct differences were observed in that in one case the peptide formed a helix prior to insertion [71] and in the other, the extended peptide inserted into the DPPC bilayer, after which it folded into a transmembrane helix [72]. These studies present an interesting comparison with our work in that they reveal the range of conformations that may be observed with membrane-associated peptides.

To our knowledge, only two computational studies have examined Aβ in a membrane-like environment. One of these, by Mobley et al. [21], examined $Aβ_{40}$ and $Aβ_{42}$ in an implicit membrane environment. Through the use of multiple Monte Carlo (MC) simulations, the authors report a number of binding modes of Aβ, each with comparable energy. The other study, by Xu et al., applied MD to studies of $Aβ_{40}$ in an explicit lipid bilayer composed of DPPC [15]. The results presented by these investigators suggest that the exit pathway of $Aβ_{40}$ from DPPC can be observed within 100 ns of MD simulation, and that much of the initial α-helicity of the peptide is maintained. Our work builds upon this previous research.

One consideration in initiating our studies was the starting conformation of $Aβ_{40}$. As we have noted, we selected a structure from an NMR study of $Aβ_{40}$ in SDS micelles. The particular structure we selected was representative of the 10 reported, and it provided us with a starting conformation in which the N-terminal portion of the peptide extended away from the DPPC bilayer. A similar conformation was used by Xu et al. in their study, and this conformation also has been used in aqueous simulations [17]. Notably, a starting structure incorporating an α-helical segment in the bilayer is reasonable considering the preponderance of this structure in single membrane-spanning protein segments. Another consideration in our studies was the composition of the lipid bilayer. Although a number of different compositions might have been chosen, we elected to use DPPC because it was used in the Xu et al. study, thereby allowing

some comparison of our work with the only other computational study of Aβ in an explicit lipid environment.

Of note is the difference between the results we present and the work presented by Xu et al. [15], which may be attributed to differences in the force fields used or the way the system was prepared. For this study, we used an updated version of the Gromos force field [44]. There are subtle differences between the force field used by Xu et al. and that of the present study. The Gromos96 53a6 parameter set contains charges that generate slightly more polar entities (Tyr, His, etc.) than in the Gromos87 force field. The Lennard–Jones parameters were also refined in Gromos96 53a6. As a result, the nature and strength of the nonbonded interactions between the peptide and the bilayer may be slightly different. The peptide in the present study may have experienced stronger interactions with lipid headgroups, preventing diffusion into the bulk solvent. In preparing the system, our methodology differed in that we created a cavity for the peptide with void space that was closed during equilibration, allowing the lipids to pack around the $A\beta_{40}$ peptide. The authors of the previous study report removing one DPPC molecule from the pre-equilibrated bilayer prior to $A\beta_{40}$ insertion. This method may have resulted in different forces between the lipids and the inserted peptide than our method.

The fact that large conformational changes in the Aβ peptide were observed in a 100-ns timeframe is not surprising, as previous aqueous MD studies have witnessed unfolding of Aβ within 10 ns using the Gromacs force field [17] and in 50 ns using Gromos96 [19]. Fibril assembly has been modeled as occurring in under 10 ns with the Amber94 and Charmm27 force fields [18], and Aβ oligomers have been assembled from peptide fragments under the Charmm and Cff91 force fields [9].

We recognize that it is not possible to comprehensively sample all possible conformations over the course of a single 100-ns MD simulation. In fact, some of the structural differences that we observed among the simulations may arise from limitations in conformational sampling rather than from the conditions imposed during the simulations. Nevertheless, reasonably consistent results were observed under some conditions, from which we were able to make some general observations.

pH effects

In simulations at physiologically-relevant pH (A1–A4, C1–C2), our results compare well with the findings of Coles et al., who in addition to reporting the structure of $A\beta_{40}$ at pH 5.1, found that at pH above 6.0, residues 15–24 of $A\beta_{40}$ were capable of assuming an unstructured conformation [14]. We found that this disorder persisted in simulations A1, A2, and A4, and there was a transient loss of helicity in this region of the peptide in simulation C1.

In each of the low-pH simulations (B1–B4), $A\beta_{40}$ retained an appreciable amount of α-helical character, except for simulation B2, which lost much of its helicity by the end of the trajectory. In the two simulations of fully-protonated $A\beta_{40}$, α-helicity was preserved in residues 25–36 in B3, and 15–36 in B4, broken only by a bend at residues 25–27. This finding suggests that protonation of acidic residues and histidines helps stabilize helical structure in the presence of a membrane. The observation regarding B4 compares exactly with the structural predictions made by Coles et al. regarding Aβ in the presence of SDS micelles, although B4 represented a system pH lower than that of all the systems tested by Coles et al. [14]. Since the two systems (SDS micelles and DPPC bilayers) differ in both surface charge and lipid composition, there must be some common feature inherent to Aβ that allows this structure to be observed.

Unwinding of $A\beta_{40}$ has been observed experimentally to be a pH-dependent process, and our simulations agree well with these observed data, in that in most of our low-pH simulations (B1–B4, where $A\beta_{40}$ was highly protonated), much of the original α-helicity was retained in the trajectory. This contrasts with the more physiologically-relevant simulations (A1–A4, C1–C2), wherein we observed a greater degree of loss of α-helicity in favor of β-structures and random coils.

Insertion depth

Models A and C in this study modeled the Aβ peptide under comparable conditions but at two different starting locations in the DPPC bilayer (Lys-28 and Val-24 at the interface, respectively). As observed in the Model C simulations, locating Val-24 at the interface consistently caused the peptide to adopt a more transmembrane orientation. This phenomenon was observed once in the Model A series (simulation A3), but for the rest of the Model A simulations, $A\beta_{40}$ remained partially embedded, with Lys-28 at the interface. This occurrence may have been a result of two factors, the first of which is the fact that in A3, the C-terminus of the peptide was protonated, making it more hydrophobic and thus more likely to implant in the bilayer. Simulation A3 was conducted in the absence of additional ionic strength, which may be the reason for the difference between A3 and A4, both of which had protonated C-termini. A4 was simulated in the presence of ~100 mM NaCl, which may have kept the aqueous segment of the peptide from penetrating the bilayer.

Electrostatic interactions and ionic strength

In the present study, we found a number of electrostatic interactions common among all of the simulations conducted. The most notable of these were cation–π interactions, which most frequently formed between the choline headgroups and residues Phe-4, Tyr-10, Phe-19, and Phe-20. In cases where $A\beta_{40}$ embedded in the bilayer more deeply, cation–π interactions involving Phe-19 and Phe-20 were not observed, as these residues resided in the bilayer interior. Another important electrostatic interaction

involves Arg-5. This residue associated strongly with phosphate moieties of the lipid headgroups, and in some instances was found to embed into the ester region of the bilayer (A1, B3, and C2), where it remained for a significant portion of the trajectory. Aromatic interactions with lipid headgroups have been observed computationally to persist for several nanoseconds at a time, and positively-charged residues have also been found to embed themselves in the phosphate region of the bilayer [50].

The presence of a 100 mM ionic strength appeared to have little consistent effect on the properties of the peptide. In one case (A2), helix 1 of the peptide unfolded rapidly, but in another (A4), much of the helicity in this region was maintained, even after 100 ns. Helix 2 lost much of its α-helical character in both of these cases, indicating that the increased ionic strength may have had an effect on the dielectric environment near the membrane–water interface and thus the properties of the embedded helix. Simulation C2 was also conducted in the presence of ~100 mM NaCl, but exhibited no obvious differences relative to C1, conducted in the presence of only Na^+ counterions.

In all simulations, we witnessed the elongation of a disordered segment across the surface of the lipid bilayer, within the phosphatidylcholine headgroups. This segment stretched from residues 1–16, 1–24, or 1–28, depending on how far the peptide was embedded in the bilayer over time. This finding agrees with experimental observations of Yip and McLaurin [25], who found amyloid fibrils within the lipid headgroups. Also related to these findings are the results obtained by Bokvist et al. [73], who used a combination of NMR and circular dichroism spectroscopy to find that a short segment of Aβ is embedded in membranes with neutral headgroups. These investigators also found that Aβ consists of mostly β-structures at pH 7.8, with very little α-helical character. These findings correlate with our simulations A1 and A2, which utilize the same protonation state studied by Bokvist et al. [73].

For amyloid plaques to form, Aβ peptides must exit the bilayer and self-associate. We did not observe exit of the peptide from the bilayer in our simulations, and at least two factors may account for this observation. One is that the length of time of the simulations simply was not sufficient to observe this behavior of the peptide. The second is that experimental evidence indicates that a nucleation site is needed to initiate the aggregation process. Specifically, the association of Aβ with gangliosides in lipid rafts and glycosaminoglycans may be important nucleation sites for Aβ aggregation [74,75]. Perhaps Aβ in these specialized membrane regions would be more susceptible to exiting the bilayer. Future experiments and simulations will be required to address these types of issues.

Acknowledgments

The authors thank Joe Lambert for scripts and useful information regarding system preparation, Joe Allen for useful discussions regarding Gromacs, the members of the gmx-users listserv (especially Mark Abraham, Tsjerk Wassenaar, and Itamar Kass) for assistance, Sukit Leekumjorn for the use of software and advice regarding running Gromacs in parallel on SystemX, the Terascale Computing Facility at Virginia Tech for computing time and technical support, and Caroline Osborne for other useful discussions.

References

[1] A. Alzheimer, Int. J. Geriatr. Psychiatry 6 (1991) 129–130.
[2] http://www.alz.org/national/documents/Report_2007FactsAndFigures.pdf.
[3] D.J. Selkoe, Nature 399 (1999) A23–A31.
[4] S. Chimon, Y. Ishii, J. Am. Chem. Soc. 127 (2005) 13472–13473.
[5] D.M. Walsh, D.M. Hartley, Y. Kusumoto, Y. Fezoui, M.M. Condron, A. Lomakin, G.B. Benedek, D.J. Selkoe, D.B. Teplow, J. Biol. Chem. 274 (1999) 25945–25952.
[6] K. Ma, E.L. Clancy, Y. Zhang, D.G. Ray, K. Wollenberg, M.G. Zagorski, J. Am. Chem. Soc. 121 (1999) 8698–8706.
[7] D.B. Teplow, N.D. Lazo, G. Bitan, S. Bernstein, T. Wyttenbach, A. Baumketner, J.-E. Shea, B. Urbanc, L. Cruz, J. Borreguero, H.E. Stanley, Acc. Chem. Res. 39 (2006) 635–645.
[8] T. Ban, K. Yamaguchi, Y. Goto, Acc. Chem. Res. 39 (2006) 663–670.
[9] B. Ma, R. Nussinov, Proc. Natl. Acad. Sci. USA 99 (2002) 14126–14131.
[10] B. Ma, R. Nussinov, Curr. Opin. Chem. Biol. 10 (2006) 445–452.
[11] R. Tycko, Biochemistry 42 (2003) 3151–3159.
[12] A.T. Petkova, R.D. Leapman, Z. Guo, W.-M. Yau, M.P. Mattson, R. Tycko, Science 307 (2005) 262–265.
[13] R.P. Mason, J.D. Estermyer, J.F. Kelly, P.E. Mason, Biochem. Biophys. Res. Commun. 222 (1996) 78–82.
[14] M. Coles, W. Bicknell, A.A. Watson, D.P. Fairlie, D.J. Craik, Biochemistry 37 (1998) 11064–11077.
[15] Y. Xu, J. Shen, X. Luo, W. Zhu, K. Chen, J. Ma, H. Jang, Proc. Natl. Acad. Sci. USA 102 (2005) 5403–5407.
[16] I. Daidone, F. Simona, D. Roccatano, R.A. Broglia, G. Tiana, G. Colombo, A. Di Nola, Proteins 57 (2004) 198–204.
[17] E. Luttmann, G. Fels, Chem. Phys. 323 (2006) 138–147.
[18] N.-V. Buchete, R. Tycko, G. Hummer, J. Mol. Biol. 353 (2005) 804–821.
[19] D. Flöck, S. Colacino, G. Colombo, A. Di Nola, Proteins 62 (2006) 183–192.
[20] B. Tarus, J.E. Straub, D. Thirumalai, J. Am. Chem. Soc. 128 (2006) 16159–16168.
[21] D.L. Mobley, D.L. Cox, R.R.P. Singh, M.W. Maddox, M.L. Longo, Biophys. J. 86 (2004) 3585–3597.
[22] E. Tischer, B. Cordell, J. Biol. Chem. 271 (1996) 21914–21919.
[23] R.P. Mason, R.F. Jacob, M.F. Walter, P.E. Mason, N.A. Adulov, S.V. Chochina, U. Igbavboa, W.G. Wood, J. Biol. Chem. 274 (1999) 18801–18807.
[24] C.C. Curtain, F.E. Ali, D.G. Smith, A.I. Bush, C.L. Masters, K.J. Barnham, J. Biol. Chem. 278 (2003) 2977–2982.
[25] C.M. Yip, J. McLaurin, Biophys. J. 80 (2001) 1359–1371.
[26] D. Eliezer, J. Gen. Physiol. 128 (2006) 631–633.
[27] Y. Sokolov, J.A. Kozak, R. Kayed, A. Chanturiya, C. Glabe, J.E. Hall, J. Gen. Physiol. 128 (2006) 637–647.
[28] R. Kayed, Y. Sokolov, B. Edmonds, T.M. McIntire, S.C. Milton, J.E. Hall, C.G. Glabe, J. Biol. Chem. 279 (2004) 46363–46366.
[29] A. Demuro, E. Mina, R. Kayed, S.C. Milton, I. Parker, C.G. Glabe, J. Biol. Chem. 280 (2005) 17294–17300.
[30] L. Cruz, B. Urbanc, J.M. Borreguero, N.D. Lazo, D.B. Teplow, H.E. Stanley, Proc. Natl. Acad. Sci. USA 102 (2005) 18258–18263.
[31] R.A. Böckmann, A. Hac, T. Heimburg, H. Grubmüller, Biophys. J. 85 (2003) 1647–1655.

[32] J.C. Gordon, J.B. Myers, T. Folta, V. Shoja, L.S. Heath, A. Onufriev, Nucleic Acids Res. 33 (2005) W368–W371.
[33] http://biophysics.cs.vt.edu/H++/index.php.
[34] T. Kameda, S. Takada, Proc. Natl. Acad. Sci. USA 103 (2006) 17765–17770.
[35] H.A. Stern, S.E. Feller, J. Chem. Phys. 118 (2003) 3401–3412.
[36] M.F. Iozzi, M. Cossi, R. Improta, N. Rega, V. Barone, J. Chem. Phys. 124 (2006).
[37] D. van der Spoel, E. Lindahl, B. Hess, A.R. van Buren, E. Apol, P.J. Meulenhoff, D.P. Tieleman, A.L.T.M. Sijbers, K.A. Feenstra, R. van Drunen, H.J.C. Berendsen, Gromacs User Manual version 3.3, The GROMACS Development Team, Groningen, 2005.
[38] D. van der Spoel, E. Lindahl, B. Hess, G. Groenhof, A.E. Mark, H.J.C. Berendsen, J. Comput. Chem. 26 (2005) 1701–1718.
[39] http://moose.bio.ucalgary.ca/index.php?page=Structures_and_Topologies.
[40] H.J.C. Berendsen, J.P.M. Postma, W.F. van Gunsteren, A. Di Nola, J.R. Haak, J. Chem. Phys. 81 (1984) 3684–3690.
[41] D.P. Tieleman, H.J.C. Berendsen, J. Phys. Chem. 105 (1996) 4871–4880.
[42] D.P. Tieleman, S.J. Marrink, H.J.C. Berendsen, Biochim. Biophys. Acta 1331 (1997) 235–270.
[43] S.-J. Marrink, O. Berger, P. Tieleman, F. Jähnig, Biophys. J. 74 (1998) 931–943.
[44] C. Oostenbrink, A. Villa, A.E. Mark, W.F. van Gunsteren, J. Comput. Chem. 25 (2004).
[45] C. Gui, W. Zhu, G. Chen, X. Luo, O.W. Liew, C.M. Puah, K. Chen, H. Jiang, Proteins 67 (2007) 41–52.
[46] Y. Xu, F.J. Barrantes, X. Luo, K. Chen, J. Shen, H. Jiang, J. Am. Chem. Soc. 127 (2005) 1291–1299.
[47] S.A. Contera, V. Lemaître, M.R.R. de Planque, A. Watts, J.F. Ryan, Biophys. J. 89 (2005) 3129–3140.
[48] S. Esteban-Martín, J. Salgado, Biophys. J. 92 (2007) 903–912.
[49] G. van den Bogaart, N. Hermans, V. Krasnikov, A.H. de Vries, B. Poolman, Biophys. J. 92 (2007) 1598–1605.
[50] S.S. Deol, P.J. Bond, C. Domene, M.S.P. Sansom, Biophys. J. 87 (2004) 3737–3749.
[51] P.J. Bond, M.S.P. Sansom, J. Mol. Biol. 329 (2003) 1035–1053.
[52] U. Essmann, L. Perera, M.L. Berkowitz, T. Darden, H. Lee, L.G. Pedersen, J. Chem. Phys. 103 (1995) 8577–8593.
[53] T. Darden, D. York, L. Pedersen, J. Chem. Phys. 98 (1993) 10089–10092.
[54] B. Hess, H. Bekker, H.J.C. Berendsen, J.G.E.M. Fraaije, J. Comput. Chem. 18 (1997) 1463–1472.
[55] http://www.arc.vt.edu/arc/SystemX/index.php.
[56] A.K. Sum, R. Faller, J.J. de Pablo, Biophys. J. 85 (2003) 2830–2844.
[57] A.K. Sum, J.J. de Pablo, Biophys. J. 85 (2003) 3636–3645.
[58] W. Kabsch, C. Sander, Biopolymers 22 (1983) 2577–2637.
[59] E.F. Pettersen, T.D. Goddard, C.C. Huang, G.S. Couch, D.M. Greenblatt, E.C. Meng, T.E. Ferrin, J. Comput. Chem. 25 (2004) 1605–1612.
[60] M. Bachar, O.M. Becker, J. Chem. Phys. 111 (1999) 8672–8685.
[61] T.-L. Lau, E.E. Ambroggio, D.J. Tew, R. Cappai, C.L. Masters, G.D. Fidelio, K.J. Barnham, F. Separovic, J. Mol. Biol. 356 (2006) 759–770.
[62] P.J. Bond, M.S.P. Sansom, Proc. Natl. Acad. Sci. USA 104 (2007) 2631–2636.
[63] S. Dorairaj, T.W. Allen, Proc. Natl. Acad. Sci. USA 104 (2007) 4943–4948.
[64] A.C.V. Johansson, E. Lindahl, Biophys. J. 91 (2006) 4450–4463.
[65] C. Haass, D.J. Selkoe, Nat. Rev. Mol. Cell Biol. 8 (2007) 101–112.
[66] P.K. Mandal, J.W. Pettegrew, Neurochem. Res. 29 (2004) 2267–2272.
[67] M.M. Sperotto, S. May, A. Baumgaertner, Chem. Phys. Lipids 141 (2006) 2–29.
[68] M. Bachar, O.M. Becker, Biophys. J. 78 (2000) 1359–1375.
[69] D.P. Tieleman, M.S.P. Sansom, H.J.C. Berendsen, Biophys. J. 76 (1999) 40–49.
[70] S.K. Kandasamy, R.G. Larson, Biophys. J. 90 (2006) 2326–2343.
[71] W. Im, C.L. Brooks III, Proc. Natl. Acad. Sci. USA 102 (2005) 6771–6776.
[72] H. Nymeyer, T.B. Woolf, A.E. Garcia, Proteins Struct. Funct. Bioinform. 59 (2005) 783–790.
[73] M. Bokvist, F. Lindström, A. Watts, G. Gröbner, J. Mol. Biol. 335 (2004) 1039–1049.
[74] A. Kakio, S.- I. Nishimoto, K. Yanagisawa, Y. Kozutsumi, K. Matsuzaki, Biochemistry 41 (2002) 7385–7390.
[75] J. McLaurin, T. Franklin, X. Zhang, J. Deng, P.E. Fraser, Eur. J. Biochem. 266 (1999) 1101–1110.